RSC Applied Polymers

Accepted Manuscript

This article can be cited before page numbers have been issued, to do this please use: U. Aslan, M. Singh, A. Gul, J. F. Douglas and A. Karim, *RSC Appl. Polym.*, 2025, DOI: 10.1039/D5LP00116A.

ROYAL SOCIETY OF CHEMISTRY

rsc.li/RSCApplPolym

View Article Online
DOI: 10.1039/D5LP00116A

Concentric Half-Domain Spacing Morphologies and Anomalous Domain Stretching in Microwave Annealed Block Copolymer Thin Films

Ugur Aslan[1], Maninderjeet Singh[2], Akhtar Gul[1], Jack F. Douglas[3], Alamgir Karim*[2]

[1] Materials Science and Engineering, University of Houston, TX 77004

[2] William A. Brookshire Department of Chemical and Biomolecular Engineering, University of Houston, TX 77004

[3] Materials Science and Engineering Division, National Institute of Standards and Technology, Gaithersburg, MD 20899

*Corresponding author: Alamgir Karim, akarim3@central.uh.edu

Key words: Island-on-island, hole-in-hole, half domain spacing, concentric layered morphology, lamellar block copolymer thin films, microwave annealing, ultra-fast annealing

Abstract

Block copolymer (BCP) films hold significant promise for a wide array of technological applications, including nanopatterning, nanophotonics, polymer electrolytes, and optical waveguides. However, the practical realization of these applications is often hindered by the slow kinetics of the ordering of block copolymers, attributed to the inherently glassy dynamics of polymeric soft materials under standard processing conditions. The diverse range of BCP morphologies further highlights the unique self-assembly characteristics of polymeric materials. In this study, we employ a microwave annealing method that generates a high substrate heating rate (18°C/s) to rapidly order lamellar BCP thin films on a high-resistivity boron-doped silicon substrate. This substrate efficiently absorbs microwave energy, creating a rapid and substantial z-temperature gradient in the BCP film. The high-temperature annealing facilitated by

View Article Online
DOI: 10.1039/D5LP00116A

microwave heating generates $1L_0$ surface terraces made up of unconventional rim-like morphologies of $0.5L_0$ (half domain spacing) height, forming half-domain height island-on-island and hole-in-hole topographies, that we hypothesize are related to the high dynamic thru-film thickness temperature gradient. Notably, reducing substrate heating rate to 13.5°C/s only produces interesting $0.5L_0$ top surface structures. Additionally, the elevated high temperatures of microwave annealing significantly increases the vertical lamellar domain size, L_0, of the BCP film surface topography, that we believe correspond to an "intermediate segregation" regime of chain stretching. This enhancement is due to the synergy of reduced interaction parameter between blocks and improved interlayer diffusional dynamics resulting from the sharp temperature spike and rapid vitrification. These unique morphological effects, exclusive to microwave annealing, are not seen in conventional thermal or solvent annealing, and opens new avenues for microwave substrate directed self-assembly (MS-DSA) to create unique surface and internal BCP morphologies for specialized applications.

1. Introduction

It is well-known that diblock copolymers self-assemble into periodic well-defined and unique nanostructures under equilibrium conditions, with morphologies such as lamellae, cylinders, spheres, gyroids, etc., depending on the relative molar mass volume ratio of the blocks and interaction parameter, χ_{12}. Thin films can exhibit a high sensitivity to processing conditions under which self-assembly and ordering occurs, as is the case with polymer crystallinity [1]. As-cast thin films of block copolymers (BCPs) often remain in a vitrified, disordered, and nonequilibrium state after being cast from solutions in neutral or good solvents [2–5]. The BCP films typically require post-processing steps, known as "annealing", to increase the mobility of BCP chains, enough to allow them to organize into morphologies closer to their thermodynamic equilibrium state [6]. Conventional annealing methods primarily involve thermal annealing [7–10] and exposure to solvent or solvent vapor annealing [11,12]. Some additional enhancements include applied electric field [13], shearing the films[14,15], subjecting them to transient heating "cold-zone annealing" [16], laser-induced annealing,[17], mixed-solvent vapor annealing [18], solvo-thermal annealing [19], sequential annealing

View Article Online
DOI: 10.1039/D5LP00116A

[8,20] and microwave annealing [21,22]. Nonetheless, the slow kinetics, often complex and costly experimental design, and limited applicability remain as general challenges in developing the full potential of BCP films for cutting-edge nano-technological applications such as nanolithography [23], fuel cells [24,25], nanofiltration membranes [26,27], photonics [28], and dielectric polymeric capacitors [29]. At present, traditional thermal annealing remains the most widely used and scientifically important method for creating stable nanostructures in BCP thin films, even though alternate annealing methods have shown that other morphologies of great potential interest can be created by annealing the BCP films under non-equilibrium conditions.

The lamellar morphology of BCP thin films forms due to the air and substrate boundaries of the films which have preferential affinity for the blocks. Lamellae-forming BCPs traditionally create islands or holes with the dimension (height perpendicular to the plane of the film) of an equilibrium domain spacing, L_0, that is inherently determined by the average BCP molecular mass, Mn. Less studied is how the domain spacing of the thin films may also be varied by quenching the BCP films into non-equilibrium states depending on the processing method used, e.g., solvent vapor annealing (SVA), direct immersion annealing (DIA), etc. These island and hole formations in BCP thin films under equilibrium conditions are a consequence of incommensuration of film thickness as a multiple of the domain spacing, i.e. islands and holes form on the film surface of quantized depth equal to one domain spacing, $1L_0$, if the thickness (h) of the BCP thin film is not equal to an integer (n) multiple of the domain spacing, L_0, i.e. $h_o = nL_0$, for symmetric wetting of the air and substrate interfaces by one block and, ($h_o = (n+0.5)L_0$ for an asymmetric wetting which has different polymer blocks wetting at the substrate and air interface) [30,31]. The lamellar domain thickness, L_0, is comprised of layers of A-b-B:B-b-A, where b refers to block, and A,B are the block polymer components, commonly referred to as "ABBA" layered domains.

Understanding the formation of these island and hole surface structures is paramount to clearly understanding the interfacial interactions of polymer chains with the processing environment and predicting the kinetics of ordering lamellar BCP thin films by chiefly studying the film topography. Notably, a single

View Article Online
DOI: 10.1039/D5LP00116A

BCP sublayer in the typical domain thickness of L_0 contributes $0.5L_0$ height, i.e., the AB of the ABBA domain. For asymmetrically wetting, driven by selective attractive interaction of a block with substrate and lower surface tension of the other block at air interface typically, in thin BCP films, islands form when the thickness, h_0, is between $(n + 0.5)L_0 < h_0 < (n + 1)L_0$, and holes form once the thickness is between $(nL_0) < h_0 < (n + 0.5)L_0$ and vice versa for symmetric BCP thin films [32–35]. Film topography transitions from surface $1L_0$ height holes when the film thickness just exceeds the nearest commensurability criteria to progressively exhibit a narrow bi-continuous window also of $1L_0$ height structures, to $1L_0$ height islands as the film thickness approaches the next n value of commensurate thickness [30,36]. The "traditional" thermal annealing method for BCP ordering suffers from long annealing times, often ranging from hours to days, and requires high-temperature processing, above glass transition temperatures of the component blocks of BCPs, making this processing method unattractive. In these regards, microwave annealing can alleviate the drawbacks of thermal annealing. Microwave heating is widely used as an alternative to conventional thermal heating in various fields, including the food industry [37], organic synthesis [38], and catalysis [39] due to its advantages of rapid heating, economic feasibility, and high-yield, high-purity outcomes [40].

This method involves the absorption of electromagnetic radiation within the frequency range of 300 MHz to 300 GHz, situated between infrared and radio frequencies. The first reported use of microwaves in chemistry dates back to the 1970s [41]. Microwave energy absorption excites the vibrational and rotational modes of molecules in the material, which is then converted into thermal motion as the excited species relax through intermolecular collisions and other phonon modes of energy transfer [38]. Compared to traditional thermal heating, microwave heating offers benefits such as volumetric and selective heating, and faster processing times. However, it is a complex process that requires careful implementation due to the potential for destructive and constructive interference of electromagnetic radiation, which can create hot and cold spots and result in nonuniform heat distribution within the material [42].

Several studies have explored microwave annealing as a versatile method for ordering various BCP structures [21,43–47]. Pioneering work by Buriak and colleagues investigated BCP film ordering using both a

View Article Online
DOI: 10.1039/D5LP00116A

microwave oven and a microwave reactor. They demonstrated perpendicular ordering of BCPs on silicon substrates, both with and without the presence of a solvent [21,22]. For solvent-free microwave annealing, Buriak's team used BCP films sandwiched between a microwave-neutral substrate and a microwave-absorbing silicon wafer, which heated the BCP films and resulted in fast ordered structures [22]. This work established the importance of the substrate's microwave absorption properties in the annealing process.

Morris and colleagues later showed that cylinder-forming BCP thin films could be ordered using a microwave reactor with a neutral brush grafted on the silicon wafer, concluding that graphoepitaxy and microwave annealing are compatible [48]. Vogt and coworkers further highlighted the significance of the position and orientation of the target material, in this case, thin films, within the commercial microwave chamber, as well as the properties of the microwave energy, to achieve ordered cylindrical BCP films [49].

Although previous studies have not addressed the scalability of this method, microwave annealing of BCP thin films appears to be a rapid, reliable, and cost-effective processing technique. In principle, BCP films should achieve similar results with microwave annealing in seconds, compared to days with conventional annealing methods. However, the unique effects arising from the rapid thermal gradient produced during microwave interaction have not been previously reported, which we address in this article. Notably, all prior microwave annealing studies have focused on pattern formation using either cylinder-forming BCPs or vertical lamellae. In contrast, this study examines microwave-assisted parallel ordering of lamellar BCPs, their surface morphology, and the associated dynamics, which have not been previously explored.

In this study, we investigate the lamellar ordering of BCP thin films through microwave annealing at short annealing times, ranging from 5 s to 15 s. We demonstrate how the duration of microwave annealing affects the ordering of BCP thin films, resulting in unique surface topographies. Numerous studies have detailed the surface morphology formation of lamellar BCP films [50–55], with notable pioneering work by Russell et al. [35,56]. Regarding the kinetics of BCP surface topography evolution into islands and holes, Smith

View Article Online
DOI: 10.1039/D5LP00116A

et al. meticulously examined terrace formations in films with a continuous thickness gradient, allowing simultaneous study of regions with varying degrees of thickness incommensurability. They observed the formation of equilibrium islands and holes with heights equivalent to the domain size (L_0) in relation to thermal annealing time and temperature, up to 170 °C [31]. For instance, the average surface hole diameter of parallel lamella-forming polystyrene-block-poly(methyl methacrylate) (PS-b-PMMA) (25000)-(26000) g/mol, labeled as (Lml_{51}), increased up to 3 μm over 48 h and remained stable up to 100 h of thermal annealing. In contrast, microwave heating typically induces localized heating spots on the substrate, potentially creating different surface morphologies in a spatially heterogeneous manner, depending on the in-plane thermal conductivity of the substrate (see Supplementary S1). High thermal conductivity substrates, such as silicon wafers, can rapidly homogenize heating from these non-uniformly distributed hot spots. This is the case for our microwave-absorbing high-resistivity silicon wafer doped with boron (B-doped Si), among other silicon substrates. Consequently, our B-doped Si substrates induce a rapid but relatively homogeneous in-plane temperature distribution across the substrate. The novelty of the morphological BCP features reported here is primarily due to the rapid heating profile between the non-microwave-absorbing BCP film and the microwave-absorbing substrate.

Complex droplet liquid surfaces after long oven annealing time, 100 h, at 180 °C such as block copolymers in melt state, transitioning from an isotropic disordered state to anisotropic ordered state can be stacked in concentric step-layered morphology [57]. Our study reveals that BCP film morphology obtained through microwave annealing includes symmetric island-on-island and hole-in-hole structures, features not observed in traditional oven or solvent annealing processes. These ordered parallel lamellar structures form within seconds, exhibiting $0.5L_0$ height and multiple concentric boundaries (see TOC Figure). Previous studies by Willson et al. have reported regular (non-concentric) $0.5L_0$ island/hole formations using block copolymer films, such as poly(styrene-block-4-trimethylsilylstyrene) (PS-b-PTMSS), and partially epoxidized block copolymer PS-b-PEI78 (34) that were manipulated to have one neutral interface, air or substrate. Willson et al. observed the $0.5L_0$ height islands or holes during the intermediate stages of

View Article Online
DOI: 10.1039/D5LP00116A

developing $1L_0$ height islands or holes through thermal annealing of lamellar BCPs [58]. However, concentric $0.5L_0$ surface morphologies with well-developed lamellar structures have not been produced by other annealing methods to our knowledge. The average diameter of the hole-in-hole structures increased with microwave annealing time, evolving towards spinodal-like island formation at the same as-cast thickness. In contrast, traditional $1L_0$ holes transition to spinodal formations due to thickness increments of BCP films during classic thermal oven annealing [30]. The average diameter of hole-in-hole structures reached approximately 3 μm in 10 seconds and continued to increase until spinodal-like or island-like morphologies formed in 15 seconds.

Our studies also report the time evolution of enhanced lamellar domain spacing (L_0) with microwave annealing time, showing an unusually high trend in L_0 increment with microwave annealing temperature, suggesting unusual chain stretching and packing dynamics under rapidly evolving non-equilibrium conditions, which are quenched upon cooling into a glassy state. The strong segregation limit (SSL) theory predicts domain spacing, $L_0 \approx bN^{2/3}\chi^{1/6}$, which gives a weak temperature dependence via $\chi \sim 1/T$, and cannot explain our results [59]. This increment also exceeds predictions based on the coefficient of thermal expansion (CTE) for the temperature change induced by microwave annealing [60]. Notably, such anomalous domain stretching has scant literature context except for SAXS studies by Baldrian et al. [61] in a 100 mm thick (bulk) PS(40k)-b-PMMA(40k) film, in the temperature range of 150-200 ^{o}C, wherein domain spacing essentially doubled from 26nm to 52 nm. This high expansion was not observed in their lower Mw PS(4.8k)-b-PMMA(6k). They hypothesized that a temperature-dependent transition from strong to an ‘‘apparent’’ weak segregation limit (WSL) could arise in reasonable correspondence with their data. In summary, we have investigated the variations in surface morphology and domain spacing of microwave-ordered parallel lamellar BCP thin films, considering different block types, molecular mass, film thickness, and processing time.

View Article Online
DOI: 10.1039/D5LP00116A

2. Experimental Section

Microwave oven and block copolymers: The microwave oven's dimensions are 25 cm x 30 cm x 30 cm, covering a volume of approximately 15 Liter. A rotating plate is at the bottom center of the microwave oven to distribute the microwave exposure uniformly over the substrate. The PS-b-PMMA block copolymer has an average number of molecular mass, M_n = PS (25000)-b-PMMA (26000) g/mol with polydispersity index, PDI, of 1.06, M_n = PS (19500)-PMMA (17000) g/mol with PDI of 1.05, and poly(styrene)-b-poly(2-vinyl pyridine) (PS-b-P2VP) with a molecular mass, M_n, of PS(25000)-b-P2VP(25000) gram with PDI of 1.06. All BCP relative volume fractions correspond to lamellar morphology ($f_A \approx 0.5$) and are purchased from Polymer source inc. Lamellar forming block PS-b-PMMA copolymers are represented with the abbreviation lml_m where subscript m is the total molecular mass in kg/mole, for e.g., PS (25000)-b-PMMA (26000) g/mol is represented as Lml_{51}. The polymer solutions are prepared with a mass fraction of 2 % relative to the solvent, anhydrous toluene, having a 99.8 % purity. 2 mass % of PS-b-PMMA in toluene is mixed for 24 hours. The polymer is completely dissolved to obtain a clear solution, filtered using a microfilter with 40 μm pores to remove the contaminants. Thin BCP films were prepared by flow coating. Flow coating requires minute quantities of polymer solution, which is pipetted into a capillary-sized (less than 1 mm) gap between an angled glass blade and the flat silicon substrate. The glass blade moves along the substrate pulling bulk of the solution while leaving a thin layer that dries to form a solid film. The thin film thicknesses range from 30 nm to 130 nm. The solid thin films are then placed inside a conventional oven for 24 h at 50 °C to evaporate any residual solvent. The thicknesses of the BCP thin films are measured using an interferometer, FILMETRICS LS-DT2.

Substrates: Boron-doped (B-doped) silicon wafers (P-type) having a resistivity of (1-100) Ω.cm (P_H) and (0.008-0.01) Ω.cm (P_L) and antimony (Sb) doped (N-type) having a resistivity of (0.01 – 0.02) Ω.cm (N_L) were used as substrates. They were purchased from university wafer. The thickness of the boron-doped silicon wafer is 1055 μm to 1075 μm with a precision of 25 μm. The silicon wafer is cut to have a dimension of approximately 15 cm by 10 cm with three straight edges and one rounded edge (due to the original

View Article Online
DOI: 10.1039/D5LP00116A

wafer's disk-like shape). The cut B-doped silicon wafers are treated using an ultraviolet−ozone (UVO) chamber and irradiated by ultraviolet (UV) with 184.9 nm and 253.7 nm wavelengths for two hours to remove organic impurities and oxidize the surface. Microwave annealing is done using a laboratory-grade microwave oven, MTST, with a maximum power of 650 watts. BCP thin films are highly sensitive to the air, which can degrade the film before the films are ordered. So, we use an in-house ceramic vacuum chamber. The vacuum chamber is placed inside the microwave oven with the BCP thin film sample. The position of the vacuum chamber with respect to the microwave stage is fixed to ensure consistent exposure. The samples are removed immediately after the desired annealing time and cooled to room temperature by placing the wafers on an aluminum block. The BCP constituents do not significantly heat up by microwave but absorb heat directly from the microwave-absorbing substrate.

Film Characterization: The BCP thin films are investigated by Atomic Force Microscopy (AFM) using a Bruker AXS-Dimension Icon. The AFM Tapping mode is used to obtain the surface morphologies of the thin films. The height and phase images are processed using the Bruker NanoScope software to remove noise and artifacts.

Temperature measurement: The measurements are performed for the same sample sizes repeated three times, and averaged. The temperatures of the BCP thin films are measured with an infrared thermometer (IR) as soon as the microwave irradiation is completed by immediately opening the microwave oven's door. Our reported temperature should be considered as the BCP film temperature at the base on the BCP film. This is because the B-Silicon wafers showed almost the same temperature for given time without a BCP film on top, because the IR emissivity from the hot base B-Silicon wafer is minimally absorbed by the BCP film, given the film thicknesses is well below 100 nm used in the study.

On the other hand, the transient temperature gradient d(DT/h)/dt in normal to film thickness (h) direction, in the rapidly heating BCP film can be large, because of the synergy of low thermal conductivity of polymers in conjunction with small value of film thickness h in denominator. However, very advanced

View Article Online
DOI: 10.1039/D5LP00116A

metrology would be required to measure this transient temperature gradient, especially given the constraints of the microwave geometry. Even with a millisecond (ms) response GaAs fiber optic temperature sensor or even a regular thermocouple that can in fact be inserted through a top microwave port, the problem is that any reliable physical contact with force of the sensor on top of a 45 nm polymer film will compromise the film thickness locally, especially when heated from its glassy to a melt state well above Tg such as encountered in microwave annealing. Thus, it will not be an accurate measure of BCP film top surface temperature. Action at a distance dielectric fiber optic temperature sensor may work, but we do not have the resources for obtaining such a setup, and these will need extensive temperature calibration as well. Future work with collaborators will aim to develop this worth-while transient temperature gradient capability in thru-film thickness (z or h) direction.

3. Results and analyses

Concentric Islands and Holes Formation: Traditional thermal oven annealing (TA) was used to order lamellae forming 25k-26k PS-b-PMMA BCP thin films at 230 ^{o}C for 24 h in high vacuum, as a means to produce control samples with uniform isotropic heating, and compared subsequently to microwave annealed samples, wherein the B-doped Silicon substrate is the only rapid heating element producing large thermal gradient in the film thickness direction from substrate to air (presented later). Asymmetric wetting PS-b-PMMA TA films produced islands with a height of 35 nm, (L_0 -37.5 nm estimated for melt state at the annealing temperature with coefficient of thermal expansion (CTE) correction),as shown in Figure 1a. Recapping that holes should form once the film thickness h_0 is between $(nL_0) < h_0 < (n + 0.5)L_0$, with integral values of n, with experimentally determined L_0 = 37.5nm, holes formed once the as-cast film thickness, was adjusted to h_0 = 45 nm = 1.20L_0 ($1L_0 < 1.20L_0 < 1.5L_0$), h_0 = 55 nm = 1.36L_0 ($1L_0 < 1.46L_0 \sim 1.5L_0$) , and h_0 = 120 nm =3.20L_0 ($3L_0 < 3.20L_0 < 3.5L_0$) , as shown in Figure 1b, 1c, and 1d, respectively. The line profiles are drawn across the islands and holes of each AFM image to determine the domain spacing (L_0) of the films. All films showed fully grown 1L_0 height as either islands or holes as expected after annealing for 24 h at 230 ^{o}C. These confined islands and holes are consistent with the

View Article Online
DOI: 10.1039/D5LP00116A

incommensurability for the preferential affinities of the PS and PMMA blocks segregating at the interfaces as evidence of parallel-lamellar morphologies. These traditional island and hole morphologies span throughout the film surface as a single layer of either island or hole. Thin films of PS-b-PMMA (25K-26K), Lml_{51}, PS-b-PMMA (19.5K-17K), $Lml_{36.5}$, and PS-b-P2VP (25K-25K), Lml^{*}_{50}, were processing by microwave heating, and the temperatures of the B-doped high-resistivity silicon substrate were recorded as function of time (5 s, 8 s, 10 s, 12 s, 15 s, and 20 s).

The microwave electromagnetic energy coupling with the PH − type2 substrate making its temperature rise significantly in a short time (no significant amount of microwave energy is absorbed directly by the PS-b-PMMA polymer film, as tested on non-absorbing substrate), imparting mobility to the polymer chains, which resulted in their parallel lamellar ordering due to the preferential migration of the PMMA block to the SiOx layer on the substrate and PS to the air interface.

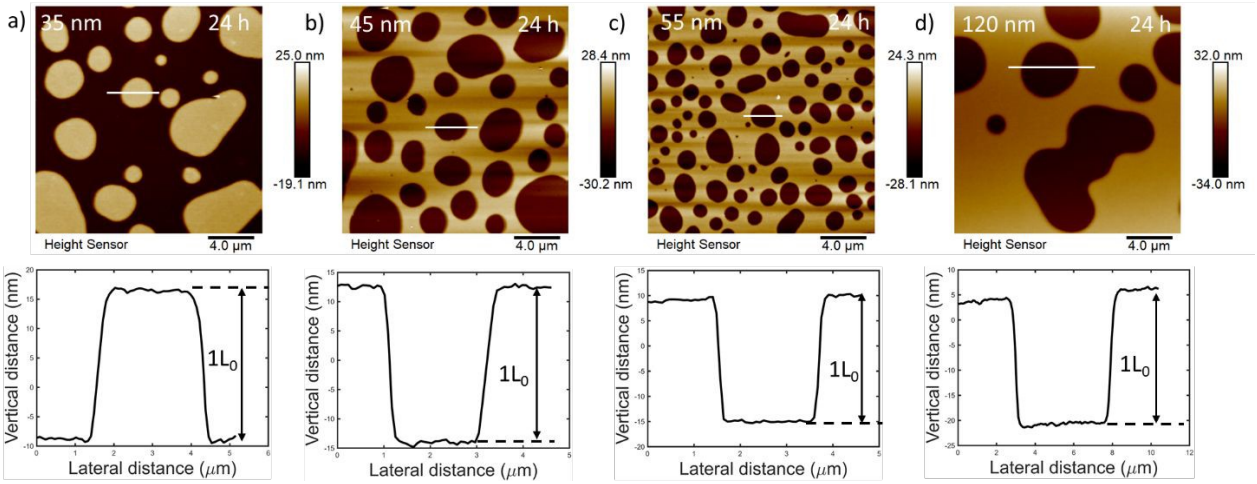

Figure 1: Thermal annealing of PS-b-PMMA thin films in traditional ovens at 230 °C and 24 h a) 35 nm b) 45 nm c) 55 nm and d) 120 nm thicknesses.

As in thermally annealed films under near-equilibrium conditions, incommensurate film thicknesses produced a surface morphology of islands and holes. The temperature, T was measured to be 85 °C at 5 s and as high as 320 °C at 20 s indicating very high heating rates, much faster than traditional vacuum thermal ovens where heating occurs mostly by conduction. The hole growth of BCP thin films is recorded for only up to 15 s with a substrate temperature of 260 °C (The films dewet after about 20 s due

View Article Online
DOI: 10.1039/D5LP00116A

to the substrate temperature reaching 320 °C, as shown in Figure 2a, we are also concerned about eventual polymer degradation). The exposure time of microwave annealing on BCP thin films is critical due to the rapid high-temperature increment, which changes their block-block thermodynamic interactions in addition to providing mobility. Microwave heating differs from traditional thermal annealing, due to the dynamic and rapid increase in temperature, for instance, 15 °C per second, while for traditional thermal annealing, the temperature increases slowly [62]. The P_H − type2 substrate heats up extremely rapidly under microwave irradiation reaching and surpassing the glass transition temperatures of PS, 100 °C, and PMMA, 115 °C blocks within 8 s of irradiation.

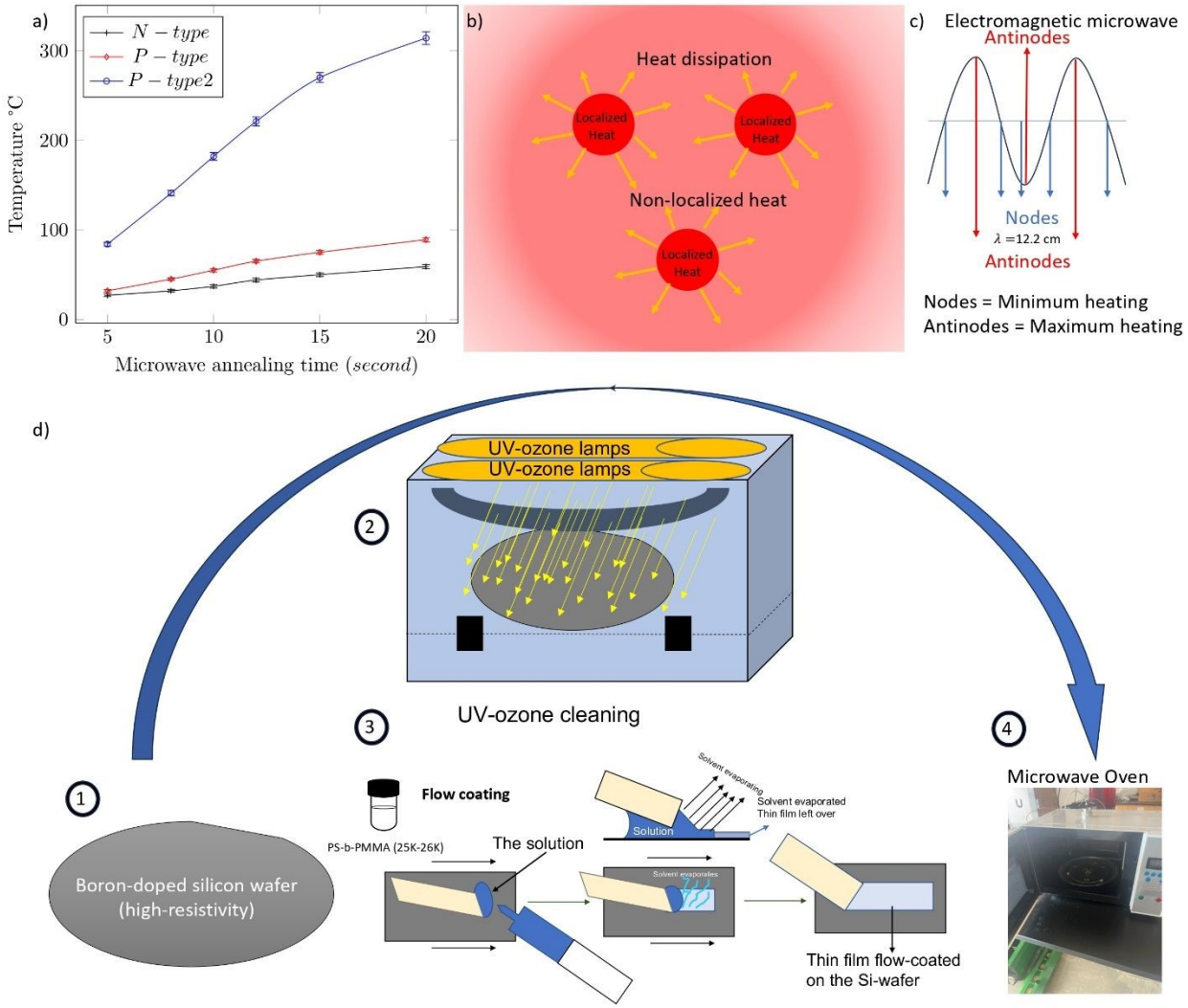

Figure 2: a) Microwave heating response of silicon wafers, P-type (low-resistivity), N-type (low-resistivity), and P-type2 (high-resistivity), b) the hypothetical heating response of the silicon wafer under

View Article Online
DOI: 10.1039/D5LP00116A

microwave radiation, c) the schematic of electromagnetic microwave radiation which heats the substrate highest at antinodes, d) the schematic of the block copolymer thin film's experimental procedure starts with the B- doped silicon wafer (≈ 15 cm x 10 cm) (1), undergoing UVO exposure (2). flow coating of the polymeric BCP solution as a thin film on the substrate (3). The sample is placed into the microwave oven (4).

This ultrafast dynamics of microwave-heated BCP thin films produces a novel surface feature of a $0.5L_0$-step height of islands and holes, surrounded by another layer step of $0.5L_0$ height islands and holes (hole-in-hole morphology is shown in Figure 3) with concentric boundaries, which we refer to as hole-in-hole and island-on-island morphologies. Since $1L_0$ is the domain spacing corresponding to ABBA, $0.5L_0$ or half-step height corresponds to only AB (i.e., single diblock, e.g., PS-b-PMMA) layer thickness. The hole-in-hole feature has a symmetric step surrounding the first hole with a very small step width (in-plane of the film) before the boundary of the second hole.

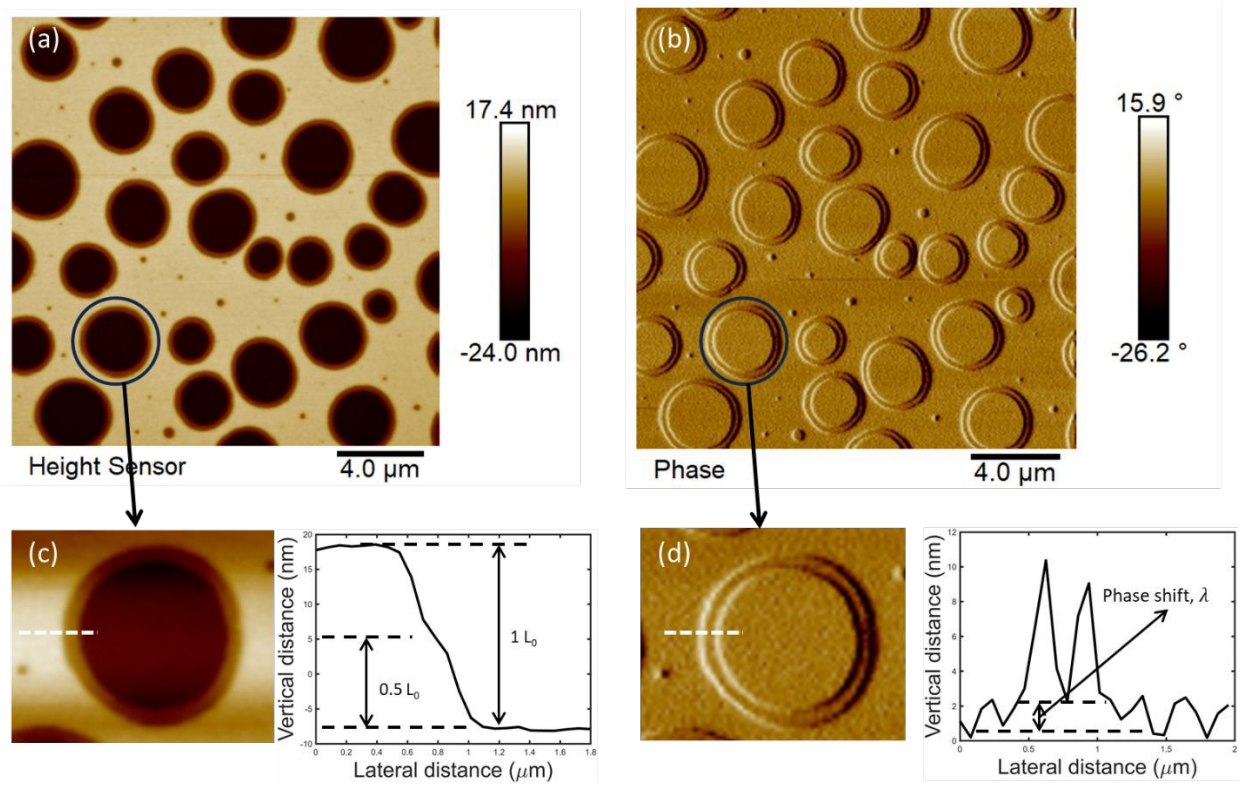

Figure 3: (a) The AFM colored height image of PS-b-PMMA showing the color of $1L_0$ with red, surface with pink and 0.5-step height with green (b) the AFM phase image of half-step lamellar domain spacing holes around one full domain spacing (c) the hole that is magnified from AFM height image and the line profile from the magnified AFM hole image (d) The AFM-phase image line profile shows the phase shift at the 0.5-step that is different from the inside of the $1L_0$ hole and the surface of the BCP thin film at 45 nm with microwave annealing at 10 s.

View Article Online
DOI: 10.1039/D5LP00116A

The AFM height image of Figure 3a with a vibrant color scale shows the height differences and step width clearly. The green rings around the solid red holes indicate the 0.5-step holes (magnified in Figure 3c). The AFM phase images show that the surface of the hole-in-hole and the bottom of the hole-in-hole morphology (domain thickness, L_0) have the same phase shift indicating the same polymer is present at the bottom and surface of the hole-in-hole of the film (Figure 3b). The phase shift, λ, from the line profile of the AFM phase image in Figure 3d shows a difference between the $0.5L_0$ step height versus other places, which are the surface and bottom of the $1L_0$ hole. The hole and the surface representing the PS have similar AFM phase angles (no phase-shift), whereas the 0.5-step height represents the PMMA has a phase shift, not to confuse with the two long sharp crests, which come from edge effects, an artifact of scanning, that is shown in Figure 3d. The magnified hole from the AFM height image indicates the line profile drawn over the edge of the hole-in-hole to show the relative heights in Figure 3c.

Figure 4 shows the change of the lamellar periodicity in the thin film starting at 5 s, continuing to 8 s, 10 s, 12 s, and 15 s, which result in higher temperatures quantified as 85 °C, 141 °C, 182 °C, 221 °C, and 270 °C, respectively. As the substrate heats up and reaches above the glass transition temperature, T_g of the blocks, the PMMA block selectively diffuses toward the SiO_2 layer. On the other hand, the PS block with lower surface energy segregates onto the air-film interface. The 5 s microwave annealing of the BCP thin film does not show any surface morphology due to insufficient substrate heating by microwave energy and the temperature remaining below the glass transition temperature of the BCP. This surface structure indicates that the BCP thin film is not yet in a fully ordered state throughout the film thickness as fully thru-thickness ordered incommensurate thickness BCP films should produce islands or holes upon parallel-lamellar ordering. As the microwave annealing time is extended, the thin film exhibits the parallel lamellar morphology shown in Figure 4 at 8 s of annealing. The total hole height (adding heights for both, barely visible, steps) on the surface of the thin film is equal to the period of the lamellar structure, $1L_0$, [63]. As the microwave exposure time increases to 10 s and 12 s, the concentric rim at $0.5\ L_0$ is observed as an inflection in the height profile, however, it appears visibly small as the line profile spans 4.5 mm, much larger that

View Article Online
DOI: 10.1039/D5LP00116A

the ~0.15 mm rim width. Upon further microwave annealing, the surface holes become progressively larger, and inter-connected, becoming similar to the spinodal-like morphology, as shown in Figure 4a, and 4b at 15 s.

Two different film thicknesses are studied in the same regime of the hole-forming degree of thickness incommensuration. The thin films with 45 nm and 55 nm thicknesses show the same trend of developing increasingly larger holes with a microwave annealing time of up to 15 s. In addition to the hole-in-hole terrace formations, when the BCP film thickness, h=35 nm, in an island formation regime, concentric island-on-island terraces are formed as shown in Figure 5a, analogous to the concentric hole-in-hole terraces of Figure 4.

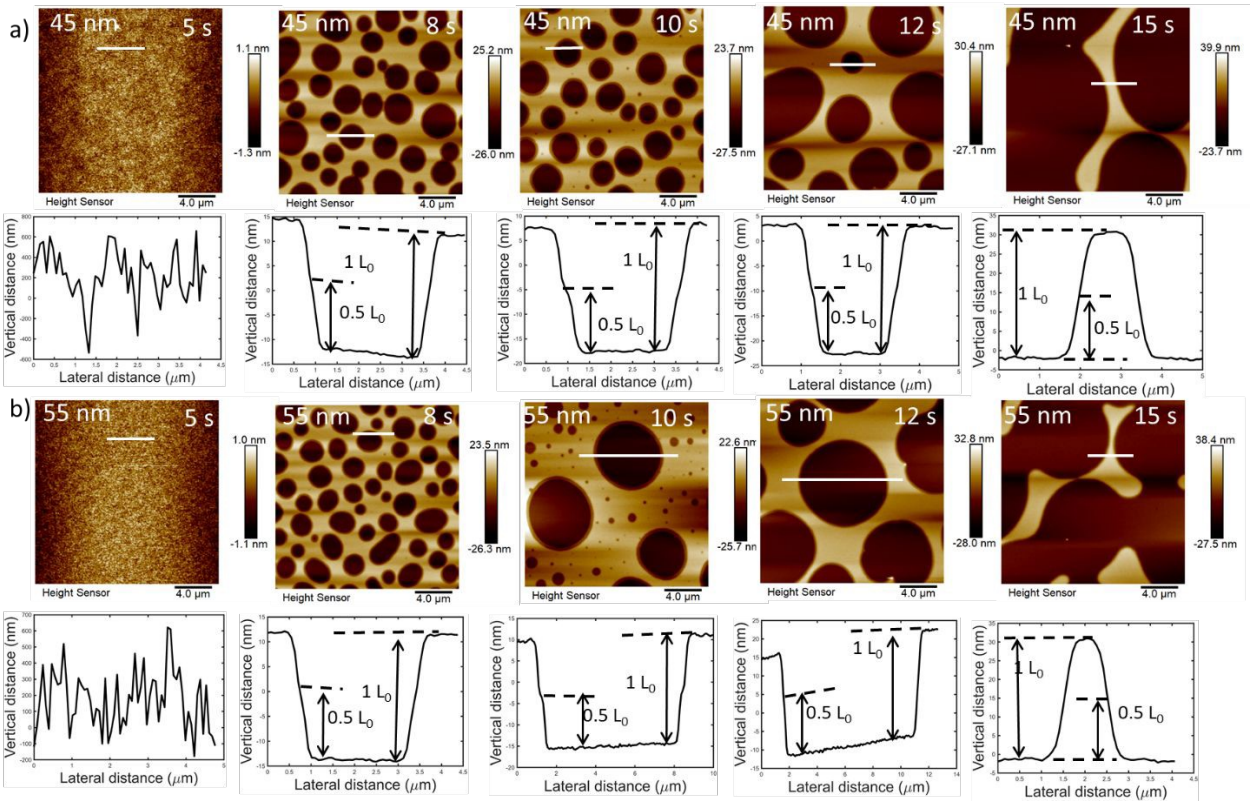

Figure 4: a,b) The microwave annealing of BCP 45 nm and 55 nm thin films are taken at 5 s, 8 s, 10 s, 12s, and 15 s: No surface holes present at 5 s, hole-in-hole terraces are created at 8 s, the average hole-in-hole diameters grow and continue at 10 s, 12 s, and holes interconnect and thus no longer exist at 15 s. The concentric terraces are more clearly observed at higher magnifications as was previously shown in **Figure 3**, but can still be seen as inflection points in these line profiles.

View Article Online
DOI: 10.1039/D5LP00116A

These islands also have two layers, each with $0.5L_0$ height, measured from the AFM height image and shown in the line height profile in Figure 5a at 35 nm. More generally, as the thickness of the BCP thin film from this island-formation regime is increased, concentric $0.5L_0$ hole-in-hole formations are observed at the cast-film thicknesses: h = 45 nm, 55 nm, and 120 nm respectively, shown as a compilation of 10 s microwave annealing time in Figure 5b, 5c, and 5d, respectively. The results indicate that the formation of quantized $0.5L_0$ height concentric terraces is not an isolated phenomenon, but a more universal feature of these BCP film system. The match of total step heights matched the long-time oven annealed L_0, provided the microwave annealing time is 8 s.

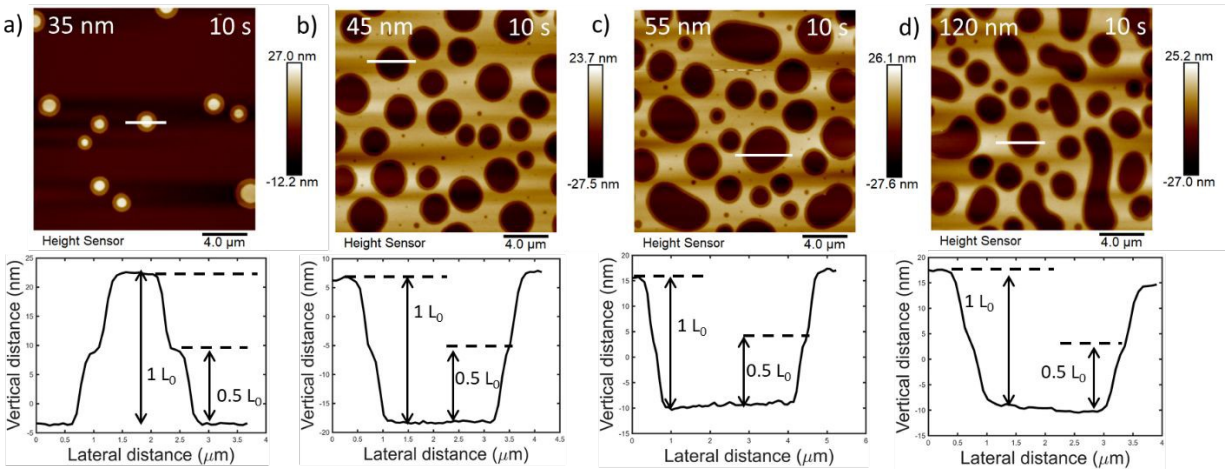

Figure 5: BCP thin films with thicknesses of 10 s microwave annealed of a) 35 nm, b) 45 nm, c) 55 nm, and d) 120 nm; island-on-island terrace formation of concentric 0.5 L_0 islands at 35 nm versus concentric 0.5 L_0 holes 45 nm, 55 nm, and 120 nm, respectively.

Anomalous PS-b-PMMA BCP Domain Stretching: Longer microwave annealing times, and with its concurrent increase of temperature, not only produce larger hole size as shown in Figure 6a, and 6b but also significantly increased overall domain spacing, L_0 (t). Figure 6a shows the change in the lamellar domain spacing of BCP thin films for as-cast film thickness h=45 nm and h=55 nm thicknesses, after microwave annealing, as inferred from AFM surface feature height, post-quenching (vitrification) to room temperature. The domain spacing, L_0 (t) as measured by the surface feature height in quenched samples, increases with the microwave annealing time, in contrast to the domain spacing during thermal oven annealing which is limited to its equilibrium value. The quenched-in lamellar domain spacing of BCP thin film increases

View Article Online
DOI: 10.1039/D5LP00116A

monotonically and substantially with increasing microwave annealing times: 8 s, 10 s, 12 s, and 15 s as shown in Figure 6a, which is correlated to the B-Silicon's rapid rise in temperature shown in Figure 2a.

This increment of the domain spacing in L_0 (33 nm @ 15s @T(t) ~ 270 °C) from L_0 (26nm @ 8s @ 181 °C) in the h=45 nm film is about 25%, which is well beyond the SSL theory prediction of ~ 10% domain swelling based on $\chi_{ps\text{-}pmma}$ (T) change (see below). Notably, Baldrian et al. [61] obtained 100% domain spacing increment in the 150-200 °C temperature window for 40k-40k PS-b-PMMA, and suggested their system was in the WSL regime. Yet, it is well known that the interfacial width of PS-b-PMMA is approximately ~5nm in this temperature window of 150-200 °C by neutron reflection and SANS, which matches well with the SSL assumption of narrow interface assumption (NIA) width.

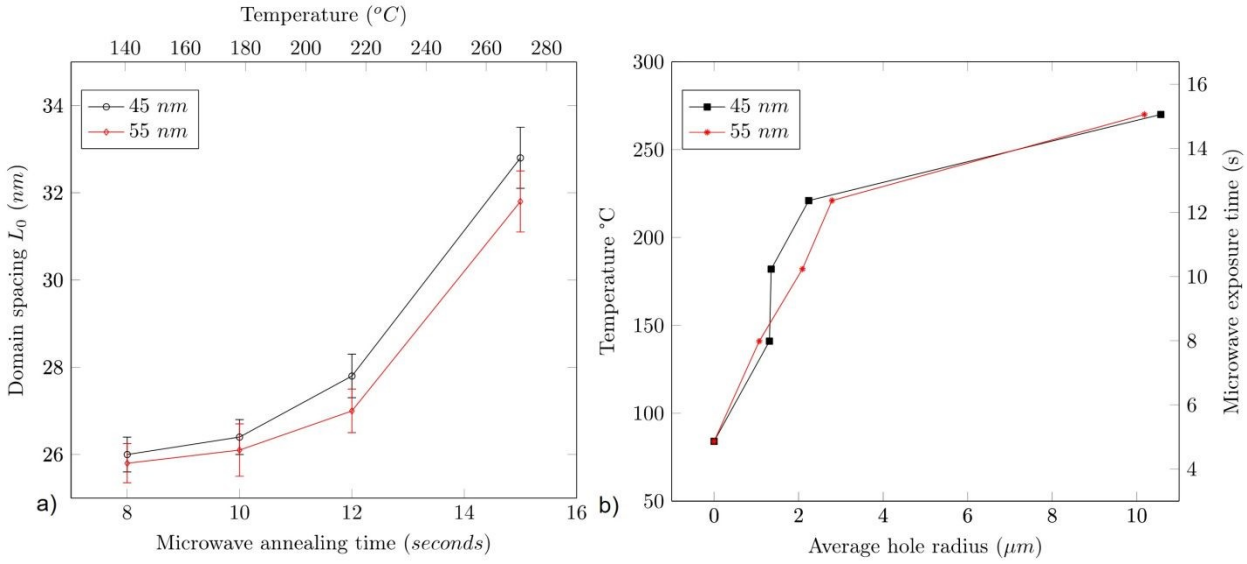

Figure 6: a) TA L_0 that is 26 nm, increases substantially for both h=45 nm and h=55 nm PS-b-PMMA films, by increasing microwave annealing time from 8 s to 15 s. See text for discussion. The corresponding temperatures of the microwave annealing time for 8 s, 10 s, 12 s, and 15 s are respectively 141 °C, 182 °C, 221 °C, and 270 °C (b) L_0 at 8 s of microwave annealing considerably increases with the increment of the microwave annealing time at 15 s.

Using the temperature dependence of $\chi_{ps\text{-}pmma}$ (T) = 0.028+3.9/T(K) [64], we obtain an estimate of $\chi_{ps\text{-}pmma}$ (@275 °C) = 0.035, and $\chi N \approx 17$ for our longest microwave annealed film of 15s. (Other forms of the temperature dependent equation for $\chi_{ps\text{-}pmma}$ (T) reported in literature do not give a significantly different value of this product, so we do not elaborate on them.) Assuming the conventional notion that $\chi N > 50$

View Article Online
DOI: 10.1039/D5LP00116A

defines SSL, and WSL by $10.495 < \chi N < 12.5$, we can conclude that our PS-b-PMMA system at the elevated temperature is in an "intermediate" segregation regime $12.5 \leq \chi N \leq 50$ rather than WSL, defined by a domain scaling that is larger than SSL (at least as per our results, and possibly Baldrian et al. (61)), but wherein interfacial widths match SSL predictions. This "intermediate segregation" and cross-over from WSL to SSL regime has been previously discussed and explored by Matsen and Bates [65,66]. Mechanistically, this is based on the temperature dependent of χ variation, possibly due to a synergistic combination of reduced enthalpic barrier since $\chi \sim 1/T$, and high entropic mobility driven by the fast diffusive motion of the chains at elevated temperatures, to easily cross between domain layers in favor of increasing interfacial chain-junction density. These elevated temperatures reduced χ and thereby interfacial tension, allowing the chains to be more fluid-like, thereby allowing them to be packed close to each other at the junctions' interface, increasing the degree of chain stretching and in turn the domain size. Such close packing would normally increase enthalpic energy per domain, but in present conditions, is balanced due to the reduced χ. Such a state of ordering may be driven by a highly non-equilibrium effect associated with an anticipated rapidly evolving spatio-temporal z-temperature gradient evolution within the confined BCP film thickness.

Notably, the percentage increase in domain size at any given microwave annealing time relative to the lowest annealing time of 8s, e.g., domain size at 15s annealing relative to 8 s is approximately the same in both films, with domain swelling ~25% for both the h=45 nm (32.6 nm @ 15 s vs 26 nm @ 8 s) and the h=55 nm (31.8 @ 15 s vs 25.7 @ 8 s) film. However absolute domain spacings appear higher in the more confined 45 nm film compared to the 55 nm film. This suggests that the relative thermal expansion as a function of temperature can be normalized by its film thickness for a more universal-like behavior, and thereby reflective of a common chain stretching molecular mechanism. The average hole diameters of Lml_{51} at 45 nm and 55 nm are also studied with annealing time and are shown in Figure 7b. The average hole radius grows steadily as the temperature increases for both thicknesses, due to the dynamic (constantly increasing) temperature increment. Notably, hole size increase kinetics in films of 45 nm versus 55 nm are roughly the same, so that "feature-size" in both out-of-plane direction (domain swelling via hole depth

View Article Online
DOI: 10.1039/D5LP00116A

kinetics data) and in-plane dimension (hole diameter expansion kinetics) have similar behavior for the two different film thicknesses.

Comparative varied substrate heating rate on BCP ordering: Figure 7a demonstrates how the temperature of the high-resistivity B-doped silicon substrate, P_H ˇtype2, changes with microwave annealing time, using two different sized substrates heated by mainly microwave energy absorption, which is proportional to substrate size, and dissipated rapidly internally by phonons (thermal conduction), which is useful to control the temperature gradient affecting the final film morphology evolution. The temperature gradient for the smaller 150 cm^2 substrate is 18 °C/s while that for the larger wafer size of 314 cm^2, it is 13.5 °C/s as shown in Figure 7b.

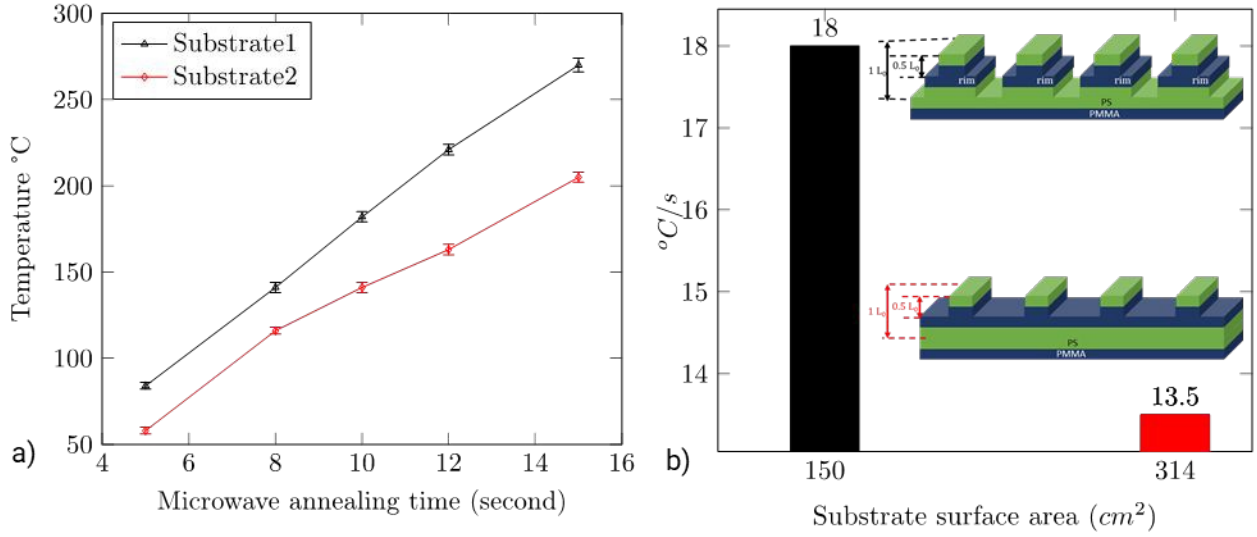

Figure 7: (a) Temperature of the BCP thin film's substrate, high-resistivity B-doped silicon wafer, P_H type2, named substrate1 and substrate2 is recorded starting from 5 s till 15 s. (b) The substrate1 which has an area of 150 cm^2 and substrate2 having 314 cm^2 showed average temperature gradients of 18 °C/s and 13.5 °C/s, respectively.

Microwave annealing of PS-b-PMMA (25K-26K) BCP thin films on substrate 2, which has a smaller temperature increase gradient of 13.5 °C/s, was also studied. Notably, the surface structures of the PS-b-PMMA on substrate2 exhibited only half-domain ($0.5L_o$) morphologies. This observation supports our hypothesis that a rapid temperature gradient sharper than 13.5 °C/s is needed at the substrate-film interface in order to create the rim-like island-on-island or hole-in-hole structures. Figure 8a shows the 45

View Article Online
DOI: 10.1039/D5LP00116A

nm thin film microwave annealed for 8 s which showed only $0.5L_0$ height holes, also shown in line height profile with heights of 12.5 nm (Figure 8a). After 15 s of microwave annealing, the BCP films still developed the $0.5L_0$ holes with an increased height of 15 nm due to attainment of higher temperature (Figure 8b). The increase in the hole heights ($0.5L_0$) is consistent with that observed during annealing on substrate1 ($1L_0$), i.e., the heating profile for our substrates shows the temporal rise of temperature for both substrates. These rates are discernably higher than the annealing rates of BCP films in traditional thermal vacuum annealing ovens.

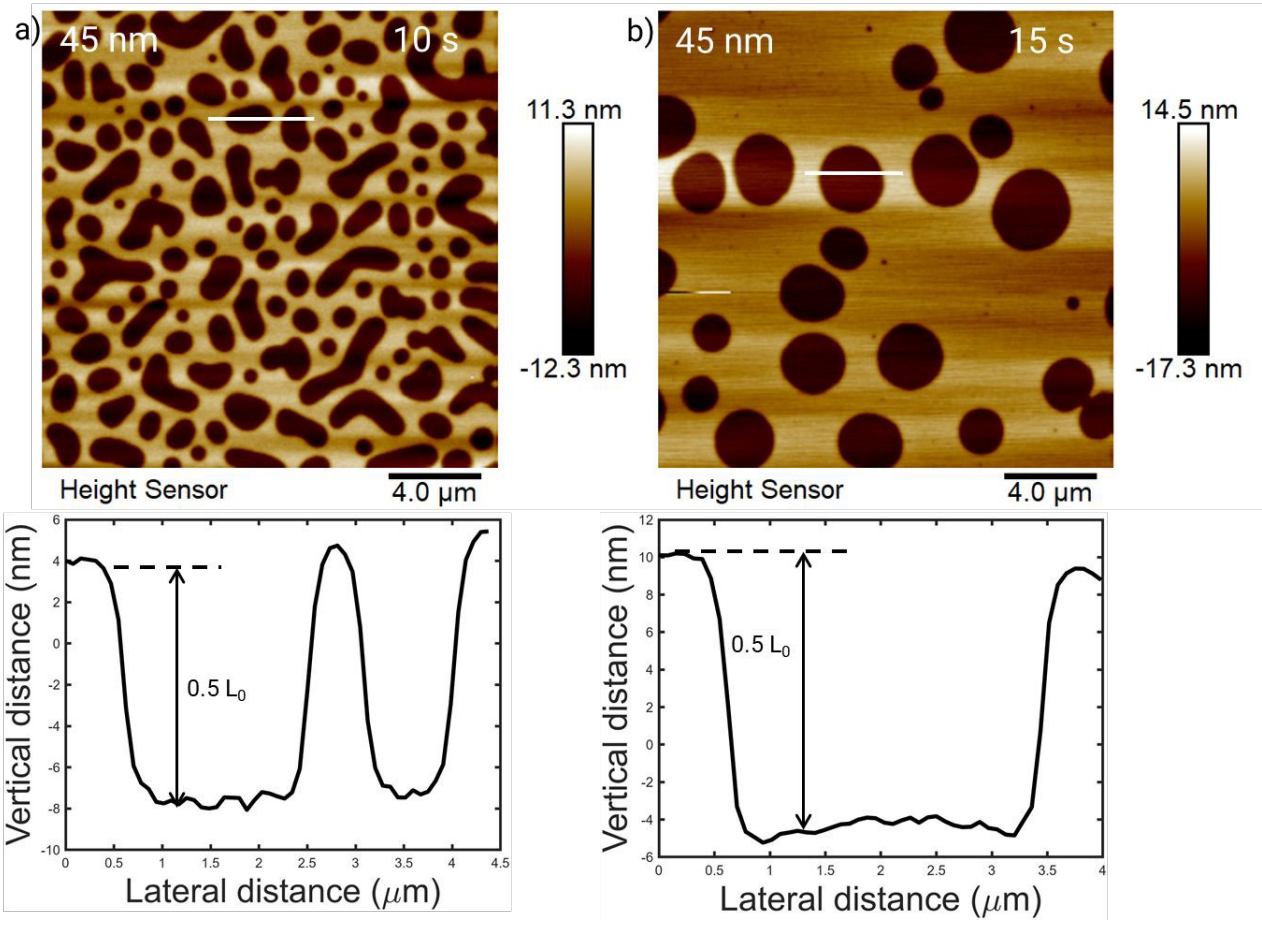

Figure 8: Surface morphology on substrate 2, with a heating rate of 13.5 °C/s, which created only $0.5L_0$ without rims for 45 nm in a) 8 s and b)15 s.

Temperature gradients with rates between 18 °C/s and 13.5 °C/s create mixed morphologies with only $0.5L_0$ islands or holes and rim-like island-on-island and hole-in-hole morphologies shown in Supplementary Information. The intermediate heating rate of the substrate rendered the BCP films to create

View Article Online
DOI: 10.1039/D5LP00116A

half-domain spacing features, islands, or holes along with island-on-island and hole-in-hole morphologies shown in Figure S6 and Figure S7, which can be attributed due to the slower temperature increment. (While outside the scope of our study, this has to do with not only substrate type, but also where microwave antinodes have highest amplitudes schematically shown in Figure 2c, which depends on substrate dimensions.) These island-on-island and hole-in-hole morphologies are also formed in $Lml_{36.5}$ thin films that make these novel features common to other molecular masses of PS-b-PMMA BCP thin films and are demonstrated in Figure S4 and S5.

For comparison, we also studied BCP PS-b-P2VP, Lml^{*}_{50} thin films with a much higher interaction parameter $\chi_{ps\text{-}p2vp} \cong 0.11$ @150 ^{o}C, annealed using microwaves for 10 s on the 18 °C/s rise substrate, however, no hole-in-hole or island-on-island features are produced due to the fact that PS and P2VP (substrate wetting) have significantly larger interfacial surface energy difference [67,68], which does not become equal (neutral at air boundary is needed for $0.5L_0$) at high temperatures like PS-b-PMMA BCP films, resulting in only $1L_0$ islands and holes shown in Figure S3. Nevertheless, the kinetics of ordering in even PS-b-P2VP BCP films on microwave-absorbing substrates is much faster than oven annealing in all cases. This suggests that concentric rim-like morphologies are prone to be observed in block copolymers having similar air interface surface energies with one block preferred at the substrate interface, under high temperature-gradient heating. Microwave processing thus provides a fast, clean, and economical method to create ordered parallel lamellar BCP thin films within seconds and with unique surface morphologies, that may be relevant to industrial processing requiring such surface morphologies such as for cheap laser light scattering standards.

4. Discussions

BCP thin films can form a variety of thermodynamic equilibrium morphologies, such as spherical, cylindrical, lamellar, and gyroid structures. These morphologies depend on the volume fractions of the constituent blocks (block A and block B, ($f_{A/B}$)), the segregation strength, χN_T [69], the degree of overall

View Article Online
DOI: 10.1039/D5LP00116A

polymerization, N_T, and the Flory-Huggins interaction parameter (χ_{AB}). Microwave annealing can sharply and rapidly increase the temperature of the underlying substrate, resulting in high-temperature gradients in the z-direction, i.e., film thickness direction. The surface structures of BCP thin films are formed due to the interactions at the free surface (top) and substrate (bottom) interfaces with the BCP thin film. Poly(styrene) (PS) and poly(methyl methacrylate) (PMMA) have similar surface energies, differing by only 0.1 dyn/cm at room temperature, with PS having the lower surface energy [70]. This difference in interfacial energies nearly vanishes at 225 °C, creating a neutral-free surface [71]. We hypothesize that the similar surface energies of PS and PMMA at high z-temperature gradient are the main reason for the creation of $0.5L_0$ step concentric morphologies, which are not observed for PS-b-P2VP (25K-25K). In $Lml_{36.5}$ BCP films, the same morphologies as in Lml_{51} are observed. We further determined that the hole-in-hole and island-on-island morphologies have the same incommensurability conditions as those of single-layered islands or hole morphologies in thermally annealed films. The total amount of polymer (block copolymer) remains constant, during the formation of the multi-tiered holes. Even in traditional "uni-depth" holes formation in ordered block copolymer thin films, the total mass of the BCP is conserved, regardless of whether they are in SSL or WSL limit. Essentially, the cumulative hole depth volumes are compensated by an elevation of the surrounding contiguous phase by an equivalent volume amount through melt diffusion-driven ordering.

We now ask the question why BCP thin films at equilibrium with non-integral thick with L_0 produce surface topographies such as island-on-island or hole-in-hole structures by microwave annealing. We hypothesize this unique rim-on-rim morphology is created in response to the steep dynamic temperature gradient in the film induced by the microwave absorbing substrate that heats the film rapidly from the bottom (B doped Si substrate only temperature rise measured to be 18 °C/s). Thus, the temperature of the BCP film at the outermost air interface is lower than in the BCP layer inner to it (that is closer to the heating substrate). This differential temperature produces a differential surface tension, which is higher at the air interface than in the layer inner to it. A higher surface tension at the air interface in turn increases

View Article Online
DOI: 10.1039/D5LP00116A

the flexural bending modulus (E) associated with the rim formation curvature at the air interface compared to the inner layer, i.e., $E_{surface} > E_{inner\ layer}$. Since flexural modulus energy varies inversely with rim radius, E~1/r, a larger rim radius at the air interface helps lower the flexural bending energy of the rim [72–74]. Regarding rim evolution kinetics, the average width of $0.5L_0$ step rims for L_0 of both 45 nm and 55 nm thicknesses decreased by 50 % with roughly doubling of microwave annealing time (from about 0.62 μm at 8 s to 0.31 μm and 0.33 μm at 15 s). Although the rims become almost indistinguishable after 15 s in the AFM height image, they are still visible in the AFM phase image (Figure S1), indicating their presence. The rim-like $0.5L_0$ structure does not disappear even at 15 seconds due to the high-temperature gradient of 18 °C/s. However, the width of the $0.5L_0$ step decreases with longer annealing times (8 s, 10 s, 12 s, and 15 s) likely due to reducing the energetically unfavorable rim surface area created, in conjunction with a z-temperature gradient homogenization with time. As surface tension depends on temperature, high-temperature gradients can, in principle, drive Marangoni patterns involving fluid flow, from higher surface tension areas (top of the film) to lower surface tension areas (bottom of the film). The Marangoni effect on simple Newtonian fluids is well studied; however, Marangoni effects are generally suppressed in high-molecular-weight polymers due to their high viscosity (75, 76). Highly stratified ordered BCP would suppress such Marangoni flow even more. Importantly, if macroscale z-directed Marangoni fluid flow occurred in these lamellar structured block copolymer films, all the individual phase-separated BCP layers would be quite mixed up from churning effects! However, we cannot rule out local molecular scale forces originating from "suppressed macroscale Marangoni effects" as causing the multi-tier surface holes [75,76].

Notably, when we use a B-doped silicon substrate that produces a lower temperature increase of 13.5 °C/s, the rim-in-rim structure disappear in favor of only a $0.5L_0$ hole morphology, consistent with Wilson's results of surface morphology evolution in incommensurate films with a neutral air interface and preferential (PMMA) substrate interface in ultrathin films. However, we did not test if our $0.5L_0$ hole morphology PS-b-PMMA films would evolve into $1L_0$ holes with extended microwave annealing time due to concerns of sample degradation beyond 15 s in air. In our case, the far from equilibrium, rapid microwave

View Article Online
DOI: 10.1039/D5LP00116A

annealing created highly stretched BCP domains in the z-direction due to the thin film confinement effects. However, we have no reason or evidence to believe that the film density below the holes layer is not the same as the bulk BCP density in this case either.

Block copolymers intrigued salient interest as materials for photonic crystals due to their ability to self-assemble, especially lamellar domains forming from block copolymer films, shown to tune optical properties. As optical implications need high-end next-generation materials, these $0.5L_0$ rim morphology can lead to the construction of optical transmission filters or waveguides [77–79]. These novel BCP morphologies with the ultra-fast annealing process also show potential implications in the internet of things (lot), gene delivery, and trapped drugs, in the hierarchical surface topographies with multi-purpose applications [74,80–82].

5. Conclusions

Microwave annealing is used to rapidly create ordered periodic parallel rim-like hole-in-hole and island-on-island lamellar nanostructures. This study thoroughly examines how temperature gradients and film thickness affect domain spacing and produce surface terraces at the interfaces of BCP thin films. By microwave absorbing B-silicon substrates @ 18 ^{o}C/s, the BCP thin films reached an equilibrium structure in as little as 8 s, forming well-developed holes on the interface, and we hypothesize a high z- temperature gradient is responsible for this first evidence of subsequent transient multilayered and concentric $0.5L_0$ surface island and hole structures that split $1L_0$ surface structure formation at higher temperature evolution up till 270 ^{o}C at 15 s. Surface energetics to reduce surface, temperature gradient homogenization and increased mobility at high temperature drive the rim widths to progressively decrease with increasing microwave annealing time. In comparison, we can achieve only $0.5L_0$ surface structures form when the substrate heating rate is 13.5 ^{o}C/s, by mechanism of neutral air and preferential substrate interactions of the BCP. Intermediate heating rates between 13.5 ^{o}C/s and 18 ^{o}C/s create mixed morphologies, so these results are highly correlated to heating rates of the substrate and the transient nature of the temperature gradient in

View Article Online
DOI: 10.1039/D5LP00116A

the film thru thickness direction. Future modeling studies can potentially lay the basis for these experimental observations, but they are out of scope of the present study.

Another unique observation is that the 15 s microwave annealing increased the domain spacing by nearly 25 % compared to the 8 s annealing, due to the concurrent lowering of interaction parameter (enthalpic effect), enhanced chain mobility and reduced penalty for stretching of polymer chains at elevated temperatures (entropic effect). We have suggested that the system lies in an "intermediate segregation" state wherein domain stretching well exceeds SSL theory, but interfacial width (as confirmed by literature) conforms to the SSL theory.

Overall, this work successfully applies microwave annealing to create hierarchical parallel lamellar morphology with interesting $0.5L_0$ rim features in vertically split $1L_0$ structures, with significantly enhanced domain spacing, by irradiating a microwave-absorbing high-resistivity B-doped silicon wafer at a high heating rate (18 ^{o}C/s). Lower heating rates conditions (13.5 ^{o}C/s) produce equally interesting $0.5L_0$ surface topography, as a simple route to attaining the uncommon $0.5L_0$ islands and holes in PS-b-PMMA BCPs. With further research aimed at scaling up the method, we suggest that microwave substrate directed self-assembly (MS-DSA) is valuable for industrial processing of BCP films for development of unique surface topography and expanded domains in the film thickness or z-dimension.

Disclaimer: Certain commercial equipment, instruments, or materials are identified in this paper to foster understanding. Such identification does not imply recommendation or endorsement by the National Institute of Standards and Technology, nor does it imply that the materials or equipment identified are necessarily the best available for the purpose.

Acknowledgments: The authors acknowledge funding from NSF (DMR) # 1900692, Welch E-2105-20220331 and Welch V-E-0003-20230731 for all aspects of this research work.

Data availability statement: The data that supports the findings of this study are available upon request

View Article Online
DOI: 10.1039/D5LP00116A

References:

1. Thurn-Albrecht T, Schotter J, Kastle GA, Emley N, Shibauchi T, Krusin-Elbaum L, et al. Ultrahigh-density nanowire arrays grown in self-assembled diblock copolymer templates. Science (1979). 2000;290(5499):2126–9.

2. Green PF, Christensen TM, Russell TP. Ordering at diblock copolymer surfaces. Macromolecules. 1991;24(1):252–5.

3. Hawker CJ, Russell TP. Block copolymer lithography: Merging “bottom-up” with “top-down” processes. MRS Bull. 2005;30(12):952–66.

4. Gu X, Gunkel I, Hexemer A, Russell TP. Controlling domain spacing and grain size in cylindrical block copolymer thin films by means of thermal and solvent vapor annealing. Macromolecules. 2016;49(9):3373–81.

5. Russell TP. X-ray and neutron reflectivity for the investigation of polymers. Materials science reports. 1990;5(4):171–271.

6. Ouk Kim S, Solak HH, Stoykovich MP, Ferrier NJ, De Pablo JJ, Nealey PF. Epitaxial self-assembly of block copolymers on lithographically defined nanopatterned substrates. Nature. 2003;424(6947):411–4.

7. Mansky P, Liu Y, Huang E, Russell TP, Hawker C. Controlling polymer-surface interactions with random copolymer brushes. Science (1979). 1997;275(5305):1458–60.

8. Sharma K, Agrawal A, Masud A, Satija SK, Ankner JF, Douglas JF, et al. Hiking down the Free Energy Landscape Using Sequential Solvent and Thermal Processing for Versatile Ordering of Block Copolymer Films. ACS Appl Mater Interfaces. 2023;15(17):21562–74.

9. Anastasiadis SH, Russell TP, Satija SK, Majkrzak CF. Neutron reflectivity studies of the surface-induced ordering of diblock copolymer films. Phys Rev Lett. 1989;62(16):1852.

10. Nowak SR, Yager KG. Photothermally directed assembly of block copolymers. Adv Mater Interfaces. 2020;7(5):1901679.

11. Kim SH, Misner MJ, Xu T, Kimura M, Russell TP. Highly oriented and ordered arrays from block copolymers via solvent evaporation. Advanced Materials. 2004;16(3):226–31.

12. Fukunaga K, Elbs H, Magerle R, Krausch G. Large-scale alignment of ABC block copolymer microdomains via solvent vapor treatment. Macromolecules. 2000;33(3):947–53.

13. Morkved TL, Lu M, Urbas AM, Ehrichs EE, Jaeger HM, Mansky P, et al. Local control of microdomain orientation in diblock copolymer thin films with electric fields. Science (1979). 1996;273(5277):931–3.

14. Qiang Z, Zhang Y, Groff JA, Cavicchi KA, Vogt BD. A generalized method for alignment of block copolymer films: solvent vapor annealing with soft shear. Soft Matter. 2014;10(32):6068–76.

View Article Online
DOI: 10.1039/D5LP00116A

15. Singh G, Yager KG, Berry B, Kim HC, Karim A. Dynamic thermal field-induced gradient soft-shear for highly oriented block copolymer thin films. ACS Nano. 2012;6(11):10335–42.

16. Singh M, Wu W, Basutkar MN, Strzalka J, Al-Enizi AM, Douglas JF, et al. Ultra-fast vertical ordering of lamellar block copolymer films on unmodified substrates. Macromolecules. 2021;54(3):1564–73.

17. Majewski PW, Yager KG. Millisecond ordering of block copolymer films via photothermal gradients. ACS Nano. 2015;9(4):3896–906.

18. Sinturel C, Vayer M, Morris M, Hillmyer MA. Solvent vapor annealing of block polymer thin films. Macromolecules. 2013;46(14):5399–415.

19. Gotrik KW, Ross CA. Solvothermal annealing of block copolymer thin films. Nano Lett. 2013;13(11):5117–22.

20. Sharma K, Singh M, Satija SK, Ankner JF, Douglas JF, Karim A. Transient Interfacial Pattern Formation in Block Copolymer Thin Films via Sequential Thermal and Solvent Immersion Annealing. ACS Appl Mater Interfaces. 2024;16(12):15569–85.

21. Zhang X, Harris KD, Wu NLY, Murphy JN, Buriak JM. Fast assembly of ordered block copolymer nanostructures through microwave annealing. ACS Nano. 2010;4(11):7021–9.

22. Jin C, Murphy JN, Harris KD, Buriak JM. Deconvoluting the mechanism of microwave annealing of block copolymer thin films. ACS Nano. 2014;8(4):3979–91.

23. Bates CM, Maher MJ, Janes DW, Ellison CJ, Willson CG. Block copolymer lithography. Macromolecules. 2014;47(1):2–12.

24. Elabd YA, Hickner MA. Block copolymers for fuel cells. Macromolecules. 2011;44(1):1–11.

25. Aslan U, Çağın T. Influence of H-Content on Thermo-Mechanical Properties of NiAl Alloys. In: Materials Science Forum. Trans Tech Publ; 2018. p. 224–8.

26. Nunes SP. Block copolymer membranes for aqueous solution applications. Macromolecules. 2016;49(8):2905–16.

27. Singh M, Agrawal A, Wu W, Masud A, Armijo E, Gonzalez D, et al. Soft-Shear-Aligned Vertically Oriented Lamellar Block Copolymers for Template-Free Sub-10 nm Patterning and Hybrid Nanostructures. ACS Appl Mater Interfaces. 2022;14(10):12824–35.

28. Lee J, Koh CY, Singer JP, Jeon S, Maldovan M, Stein O, et al. 25th anniversary article: ordered polymer structures for the engineering of photons and phonons. Advanced Materials. 2014;26(4):532–69.

29. Samant SP, Grabowski CA, Kisslinger K, Yager KG, Yuan G, Satija SK, et al. Directed self-assembly of block copolymers for high breakdown strength polymer film capacitors. ACS Appl Mater Interfaces. 2016;8(12):7966–76.

30. Smith AP, Douglas JF, Meredith JC, Amis EJ, Karim A. High-throughput characterization of pattern formation in symmetric diblock copolymer films. J Polym Sci B Polym Phys. 2001;39(18):2141–58.

View Article Online
DOI: 10.1039/D5LP00116A

31. Smith AP, Sehgal A, Douglas JF, Karim A, Amis EJ. Combinatorial mapping of surface energy effects on diblock copolymer thin film ordering. Macromol Rapid Commun. 2003;24(1):131–5.

32. Maher MJ, Self JL, Stasiak P, Blachut G, Ellison CJ, Matsen MW, et al. Structure, Stability, and Reorganization of 0.5 L 0 Topography in Block Copolymer Thin Films. ACS Nano. 2016;10(11):10152–60.

33. Maher MJ, Bates CM, Blachut G, Sirard S, Self JL, Carlson MC, et al. Interfacial design for block copolymer thin films. Chemistry of Materials. 2014;26(3):1471–9.

34. Kim S, Bates CM, Thio A, Cushen JD, Ellison CJ, Willson CG, et al. Consequences of surface neutralization in diblock copolymer thin films. ACS Nano. 2013;7(11):9905–19.

35. Coulon G, Collin B, Ausserre D, Chatenay D, Russell TP. Islands and holes on the free surface of thin diblock copolymer films. I. Characteristics of formation and growth. Journal de physique. 1990;51(24):2801–11.

36. Smith AP, Douglas JF, Amis EJ, Karim A. Effect of temperature on the morphology and kinetics of surface pattern formation in thin block copolymer films. Langmuir. 2007;23(24):12380–7.

37. Sutton WH. Microwave processing of materials. MRS Bull. 1993;18(11):22–9.

38. Horikoshi S, Serpone N. Microwave frequency effect (s) in organic chemistry. Mini Rev Org Chem. 2011;8(3):299–305.

39. Palma V, Barba D, Cortese M, Martino M, Renda S, Meloni E. Microwaves and heterogeneous catalysis: A review on selected catalytic processes. Catalysts. 2020;10(2):246.

40. Adam D. Microwave chemistry: Out of the kitchen. Nature. 2003;421(6923):571–3.

41. Liu SW, Wightman JP. Decomposition of simple alcohols, ethers and ketones in a microwave discharge. Journal of Applied Chemistry and Biotechnology. 1971;21(6):168–72.

42. Campanone LA, Zaritzky NE. Mathematical analysis of microwave heating process. J Food Eng. 2005;69(3):359–68.

43. Toolan DTW, Adlington K, Isakova A, Kalamiotis A, Mokarian-Tabari P, Dimitrakis G, et al. Selective molecular annealing: in situ small angle X-ray scattering study of microwave-assisted annealing of block copolymers. Physical Chemistry Chemical Physics. 2017;19(31):20412–9.

44. Mokarian-Tabari P, Cummins C, Rasappa S, Simao C, Sotomayor Torres CM, Holmes JD, et al. Study of the kinetics and mechanism of rapid self-assembly in block copolymer thin films during solvo-microwave annealing. Langmuir. 2014;30(35):10728–39.

45. Higuchi T, Shimomura M, Yabu H. Reorientation of microphase-separated structures in water-suspended block copolymer nanoparticles through microwave annealing. Macromolecules. 2013;46(10):4064–8.

46. Borah D, Shaw MT, Holmes JD, Morris MA. Sub-10 nm feature size PS-b-PDMS block copolymer structures fabricated by a microwave-assisted solvothermal process. ACS Appl Mater Interfaces. 2013;5(6):2004–12.

View Article Online
DOI: 10.1039/D5LP00116A

47. Shi X, Wang X, Wang Y, Wang Y. Producing nanoporosities in block copolymers within 30 s by microwave-boosted selective swelling. Macromolecules. 2020;53(9):3619–26.

48. Borah D, Senthamaraikannan R, Rasappa S, Kosmala B, Holmes JD, Morris MA. Swift nanopattern formation of PS-b-PMMA and PS-b-PDMS block copolymer films using a microwave assisted technique. ACS Nano. 2013;7(8):6583–96.

49. Qiang Z, Ye C, Lin K, Becker ML, Cavicchi KA, Vogt BD. Evolution in surface morphology during rapid microwave annealing of PS-b-PMMA thin films. J Polym Sci B Polym Phys. 2016;54(15):1499–506.

50. Park S, Stoykovich MP, Ruiz R, Zhang Y, Black CT, Nealey PF. Directed assembly of lamellae-forming block copolymers by using chemically and topographically patterned substrates. Advanced Materials. 2007;19(4):607–11.

51. Liu CC, Ramírez-Hernández A, Han E, Craig GSW, Tada Y, Yoshida H, et al. Chemical patterns for directed self-assembly of lamellae-forming block copolymers with density multiplication of features. Macromolecules. 2013;46(4):1415–24.

52. Kim S, Nealey PF, Bates FS. Directed assembly of lamellae forming block copolymer thin films near the order–disorder transition. Nano Lett. 2014;14(1):148–52.

53. Welander AM, Kang H, Stuen KO, Solak HH, Müller M, de Pablo JJ, et al. Rapid directed assembly of block copolymer films at elevated temperatures. Macromolecules. 2008;41(8):2759–61.

54. Kim SO, Kim BH, Kim K, Koo CM, Stoykovich MP, Nealey PF, et al. Defect structure in thin films of a lamellar block copolymer self-assembled on neutral homogeneous and chemically nanopatterned surfaces. Macromolecules. 2006;39(16):5466–70.

55. Heier J, Kramer EJ, Groenewold J, Fredrickson GH. Kinetics of individual block copolymer island formation and disappearance near an absorbing boundary. Macromolecules. 2000;33(16):6060–7.

56. Thurn-Albrecht T, Steiner R, DeRouchey J, Stafford CM, Huang E, Bal M, et al. Nanoscopic templates from oriented block copolymer films. Advanced Materials. 2000;12(11):787–91.

57. Croll AB, Massa M V, Matsen MW, Dalnoki-Veress K. Droplet shape of an anisotropic liquid. Phys Rev Lett. 2006;97(20):204502.

58. Maher MJ, Self JL, Stasiak P, Blachut G, Ellison CJ, Matsen MW, et al. Structure, Stability, and Reorganization of 0.5 L0 Topography in Block Copolymer Thin Films. ACS Nano [Internet]. 2016 Nov 22;10(11):10152–60. Available from: https://doi.org/10.1021/acsnano.6b05390

59. Bates FS, Fredrickson GH. Block copolymer thermodynamics: theory and experiment. Annu Rev Phys Chem. 1990;41(1):525–57.

60. Pochan DJ, Lin EK, Satija SK, Wu W li. Thermal expansion of supported thin polymer films: A direct comparison of free surface vs total confinement. Macromolecules. 2001;34(9):3041–5.

61. Holoubek J, Lednický F, Baldrian J. Non-equilibrium self-assembled structures in thick PS-b-PMMA copolymer films. Eur Polym J. 2006;42(10):2236–46.

View Article Online
DOI: 10.1039/D5LP00116A

62. Thostenson ET, Chou T. Microwave and conventional curing of thick-section thermoset composite laminates: experiment and simulation. Polym Compos. 2001;22(2):197–212.

63. Masud A, Wu W, Singh M, Tonny W, Ammar A, Sharma K, et al. Solvent processing and ionic liquid-enabled long-range vertical ordering in block copolymer films with enhanced film stability. Macromolecules. 2021;54(18):8512–25.

64. Russell TP, Hjelm Jr RP, Seeger PA. Temperature dependence of the interaction parameter of polystyrene and poly (methyl methacrylate). Macromolecules. 1990;23(3):890–3.

65. Matsen MW, Bates FS. Unifying weak-and strong-segregation block copolymer theories. Macromolecules. 1996;29(4):1091–8.

66. Matsen MW, Bates FS. Block copolymer microstructures in the intermediate-segregation regime. J Chem Phys. 1997;106(6):2436–48.

67. Ji S, Liu CC, Son JG, Gotrik K, Craig GSW, Gopalan P, et al. Generalization of the use of random copolymers to control the wetting behavior of block copolymer films. Macromolecules. 2008;41(23):9098–103.

68. Sauer BB, Dee GT. Surface tension and melt cohesive energy density of polymer melts including high melting and high glass transition polymers. Macromolecules. 2002;35(18):7024–30.

69. Bates FS, Fredrickson GH. Block copolymers-designer soft materials. Phys Today. 2000;52.

70. Russell TP, Coulon G, Deline VR, Miller DC. Characteristics of the surface-induced orientation for symmetric diblock PS/PMMA copolymers. Macromolecules. 1989;22(12):4600–6.

71. Mansky P, Russell TP, Hawker CJ, Mays J, Cook DC, Satija SK. Interfacial segregation in disordered block copolymers: effect of tunable surface potentials. Phys Rev Lett. 1997;79(2):237.

72. Bergeron V, Jimenez-Laguna AI, Radke CJ. Hole formation and sheeting in the drainage of thin liquid films. Langmuir. 1992;8(12):3027–32.

73. Sharp JS, Thomas KR, Weir MP. Mechanically driven wrinkling instability in thin film polymer bilayers. Physical Review E—Statistical, Nonlinear, and Soft Matter Physics. 2007;75(1):011601.

74. Holmes DP. Elasticity and stability of shape-shifting structures. Curr Opin Colloid Interface Sci. 2019;40:118–37.

75. Sternling CV and, Scriven LE. Interfacial turbulence: hydrodynamic instability and the Marangoni effect. AIChE Journal. 1959;5(4):514–23.

76. Scriven LE, Sternling C V. The marangoni effects. Nature. 1960;187(4733):186–8.

77. Fan Y, Walish JJ, Tang S, Olsen BD, Thomas EL. Defects, solvent quality, and photonic response in lamellar block copolymer gels. Macromolecules. 2014;47(3):1130–6.

78. Deng T, Chen C, Honeker C, Thomas EL. Two-dimensional block copolymer photonic crystals. Polymer (Guildf). 2003;44(21):6549–53.

View Article Online
DOI: 10.1039/D5LP00116A

79. Yoon J, Lee W, Thomas EL. Self-assembly of block copolymers for photonic-bandgap materials. MRS Bull. 2005;30(10):721–6.

80. Park K, Jin HM, Kwon K, Kim JH, Yun H, Han KH, et al. Large-Area Alignment of Supramolecular Columns by Photothermal Laser Writing. Advanced Materials. 2020;32(36):2002620.

81. Kim JH, Jeon S, In JH, Nam S, Jin HM, Han KH, et al. Nanoscale physical unclonable function labels based on block copolymer self-assembly. Nat Electron. 2022;5(7):433–42.

82. Yang GG, Choi HJ, Li S, Kim JH, Kwon K, Jin HM, et al. Intelligent block copolymer self-assembly towards IoT hardware components. Nature Reviews Electrical Engineering. 2024;1(2):124–38.

View Article Online
DOI: 10.1039/D5LP00116A

The data supporting this article have been included as part of the Supplementary Information.